

ATMOSPHERIC COMPOSITION BEYOND THE C/O RATIO

NÉSTOR ESPINOZA^{1,2}, JONATHAN J. FORTNEY³, YAMILA MIGUEL⁴

¹Instituto de Astrofísica, Facultad de Física, Pontificia Universidad Católica de Chile, Av. Vicuña Mackenna 4860, 782-0436 Macul, Santiago, Chile.

²Millennium Institute of Astrophysics, Av. Vicuña Mackenna 4860, 782-0436 Macul, Santiago, Chile.

³Department of Astronomy and Astrophysics, University of California, Santa Cruz, USA.

⁴Laboratoire Lagrange, UMR 7293, Université de Nice-Sophia Antipolis, CNRS, Observatoire de la Côte d’Azur, Blvd de l’Observatoire, CS 34229, 06304 Nice cedex 4, France.

ABSTRACT

C/O ratios have been extensively studied in the exoplanet community because they leave very specific imprints in the observed atmospheres, which can in turn help trace the formation and accretion paths of the exoplanets under study. However, it might be possible for other observable elements on exoplanet atmospheres such as Na, K, Ti, V and Fe to leave their own imprints in the atmospheres of giant, close-in exoplanets if they accrete their atmospheres in-situ, due to the fact that the condensation fronts of the compounds bearing those elements are in the interior parts of protoplanetary disks, at distances < 0.1 AU. Using chemical equilibrium calculations coupled with simple time varying physical models of protoplanetary disks, here we study variations in the ratios on the mentioned elements and whether or not these can be detected in transmission spectra of exoplanets. We show that for in-situ gas giant atmospheric accretion, these elements do leave imprints on the atmospheres of exoplanets that might be detectable by future instruments and observatories such as the future James Webb Space Telescope (JWST).

Keywords: exoplanets, atmospheres, planet formation

1. INTRODUCTION

The composition of the atmospheres of giant planets does not have to reflect the composition of their parent star. Because the atmosphere of these planets have been mostly accreted from the initial protostellar nebula, their composition is instead defined by the position of the planet in the (physically and chemically evolving) protoplanetary disk, which in turn defines how much of each element is available in solid and gas form, which the planet accretes in different ways due to the fact that the gas and the solids are decoupled from one another. This fact has been one of the key arguments in order to link planet formation and the composition of giant planet atmospheres (see, e.g., Madhusudhan et al. 2011; Öberg et al. 2011).

Because of their large observational effects on exoplanet atmospheres, C/O ratios have been precious quantities ought to be extracted from observations, specially for close-in giant exoplanets, where water features in the infrared seem to disappear for $C/O \gtrsim 1$ according to chemical equilibrium calculations (Madhusudhan 2012). This fact has led the way in order to search for such features in transmission spectra, because the pres-

ence of a water feature could then define a low C/O ratio in those hot exoplanet atmospheres. However, due to the presence of clouds, the extraction of C/O ratios is a very challenging problem (Sing et al. 2016). In fact, to date the only exoplanet for which a C/O ratio larger than 1 can be ruled out at 3σ confidence is WASP-12b Kreidberg et al. (2015).

With upcoming missions such as the James Webb Space Telescope (JWST), which promises exceptional precisions for transmission spectroscopy, it is timely to ask whether other elements could also leave their own fingerprints in the atmospheres of these giant exoplanets depending on where their atmospheres were accreted. Elements observed so far in exoplanet atmospheres are Na and K (see, e.g., Sing et al. 2016), with tentative detections of Ti, V and Fe also been published in the literature (Evans et al. 2016). However, all these elements condense very close to the parent star in a protoplanetary disk, at distances $\lesssim 0.1$ AU, which in turn means that in order to study the possible impact of these compounds on the atmospheres of giant exoplanets, we must study the physical and chemical evolution of the protoplanetary disk in this interior region. Of course, this also implies that in order for us to see an impact in the

composition of the atmosphere of a giant exoplanet, the planet has to accrete a large amount of its atmosphere in this interior part of the protoplanetary disk. Such “in-situ” accretion has indeed been recently proposed to be responsible for a substantial fraction of the so-called “hot-Jupiters” (planets with periods shorter than ~ 10 days), which reside in this interior part of the disk (Batygin et al. 2015; Boley et al. 2016) and, as such, fingerprints of the mentioned elements in the atmospheres of these giant exoplanets could in fact be used as tests for this proposed model of gas giant formation.

The aim of this work is to study whether these elements leave signatures that we can detect with the precisions of future instruments such as the future JWST. The paper is structured as follows. In Section 2, we detail our model calculations with which we study the condensation fronts of the different Na, K, Ti, V and Fe-bearing compounds using chemical equilibrium calculations coupled with a simple time-dependant 1D+D physical model for the protoplanetary disk. In 3 we use models for solid and gas accretion in order to track the accretion history of simulated planets, and study how these translate to observables in the transmission spectrum of the exoplanets. In 4 we discuss our results and in 5 we present our conclusions and future work.

2. PROTOPLANETARY DISK MODEL

2.1. Physical model for the Protoplanetary disk

In order to be able to perform fast calculations of the temperature and pressure profile in the protoplanetary disk as a function of radius, we decided to use the simple analytic model proposed by Chambers (2009). This model is a 1D+D model which allows to compute the evolution of a viscous, irradiated disk as a function of the distance to the parent star. In brief, the idea of the model is to note that a disk is not only heated by viscous interactions but, because it has a vertical extension which is not negligible in the outer portions of the disk, it can also be heated by direct radiation from the star impacting the disk. As such, the model defines that there are two major zones in a protoplanetary disk: an inner zone where viscous heating dominates the evolution of the disk (where the vertical extension is negligible, and, thus, stellar irradiation doesn’t greatly affect the evolution of the disk) and an outer zone which, because it is more extended in vertical extent, captures stellar radiation which defines its evolution. In practice, the disk is divided in three regions: the interior part, dominated by viscous heating, the outer part, dominated by stellar irradiation, and a transition zone which contains a mixture of both contributions.

Table 1. Parameters of the Chambers (2009) 1D+D protoplanetary disk model

Parameter	Description	Adopted value
T_s	Stellar temperature	4200 K
M_0	Initial mass of the disk	$0.1M_\odot$
R_s	Stellar radius	$3R_\odot$
s_0	Initial radius of disk’s outer edge	33 AU
k_0	Opacity	$3 \text{ cm}^2/\text{g}$
α	Viscosity parameter	10^{-2}
μ	Mean molecular weight	2.4
γ	Adiabatic index	1.4
T_e	Temperature of solid evaporation	1380 K

NOTE—Parameter values taken to match a Protoplanetary disk similar to the one that generated the Solar System.

The Chambers (2009) model gives the temperature and surface density as a function of radius given the 9 parameters defined in Table 1, which span both stellar parameters and the initial and physical properties of the disk. With these, and defining

$$\Omega_0 = \sqrt{\frac{GM_s}{s_0^3}},$$

$$\begin{aligned} \Sigma_{\text{vis}} &= \frac{7M_0}{10s_0^2}, \\ T_{\text{vis}} &= \left(\frac{27k_0}{64\sigma}\right)^{1/3} \left(\frac{\alpha\gamma k_B}{\mu m_H}\right)^{1/3} \Sigma_{\text{vis}}^{2/3} \Omega_0^{1/3}, \\ T_{\text{rad}} &= (4/7)^{1/4} \left(\frac{T_s k_b R_s}{GM_s \mu m_H}\right)^{1/7} \left(\frac{R_s}{s_0}\right)^{3/7} T_s, \end{aligned}$$

$$\begin{aligned}\tau_{\text{vis}} &= \frac{1}{16\pi} \frac{\mu m_H}{\alpha \gamma k_B} \frac{\Omega_0 M_0}{\Sigma_{\text{vis}} T_{\text{vis}}}, \\ \Sigma_{\text{evap}} &= \Sigma_{\text{vis}} \left(\frac{T_{\text{vis}}}{T_e} \right)^{14/19}, \\ \Sigma_{\text{rad}} &= \Sigma_{\text{vis}} \frac{T_{\text{vis}}}{T_{\text{rad}}},\end{aligned}$$

the model gives the temperature and surface density as a function of distance to the parent star r and time t as follows. For radii smaller than

$$r_e = s_0 \left(\frac{\Sigma_{\text{evap}}}{\Sigma_{\text{vis}}} \right)^{95/63} (1 + t/\tau_{\text{vis}})^{-19/36},$$

the temperature and surface density are defined by viscous heating, and are given by

$$\begin{aligned}T(r) &= T_{\text{vis}}^{5/19} T_e^{14/19} \left(\frac{r}{s_0} \right)^{-9/38} (1 + (t/\tau_{\text{vis}})^{-1/8}), \\ \Sigma(r) &= \Sigma_{\text{evap}} \left(\frac{r}{s_0} \right)^{-24/19} (1 + t/\tau_{\text{vis}})^{-17/16}.\end{aligned}$$

For radii larger than r_e but smaller than

$$r_o = s_0 \left(\frac{\Sigma_{\text{rad}}}{\Sigma_{\text{vis}}} \right)^{70/33} (1 + t/\tau_{\text{vis}})^{-133/132},$$

we are in the transition zone, and the temperature and surface density are given by

$$\begin{aligned}T(r) &= T_{\text{vis}} \left(\frac{r}{s_0} \right)^{-9/10} (1 + (t/\tau_{\text{vis}})^{-19/40}), \\ \Sigma(r) &= \Sigma_{\text{vis}} \left(\frac{r}{s_0} \right)^{-3/5} (1 + t/\tau_{\text{vis}})^{-57/80}.\end{aligned}$$

Finally, for radii larger than r_o , we are in the part of the disk that is heated by stellar radiation, and the temperature and surface density are given by

$$\begin{aligned}T(r) &= T_{\text{rad}} \left(\frac{r}{s_0} \right)^{-3/7}, \\ \Sigma(r) &= \Sigma_{\text{rad}} \left(\frac{r}{s_0} \right)^{-15/14} (1 + t/\tau_{\text{vis}})^{-19/16}.\end{aligned}$$

Figure 1 shows the resulting profiles using the parameters listed in Table 1, which are the parameters that are close to what it is expected for a protoplanetary disk such as the one that formed our Solar System, and which we use in this work.

2.2. Chemical evolution of the protoplanetary disk

Modelling the chemical evolution of protoplanetary disks is, in general, a complex task due to non-equilibrium reactions taking part on most of the disk (see, e.g., Lodders 2010; Henning & Semenov 2013). In this work, however, we are mainly interested in the inner regions of the disk, where Na, K, Ti, V, and Fe-bearing elements condense, which occurs at temperatures ~ 1000 K (Lodders 2003), or at distances $\lesssim 0.1$ AU. In this hot part of the disk, equilibrium conditions might be attained quicker than in the outer parts of the disk and because of this in this work we make the simplifying assumption of chemical equilibrium in this region of the disk.

In order to perform our chemical equilibrium calculations, we use the Chemical Equilibrium with Applications (CEA) NASA code, which is publicly available in the web¹. CEA performs chemical equilibrium calculations by minimizing the Gibbs free energy of the compounds under consideration given a pressure and temperature, and has an extensive library of elements, being able to handle elements in gas, liquid or solid phases. New compounds can also be added if one has the entropy, enthalpy and specific heat at constant pressure in polynomial form, which might be obtained from experimental data.

Performing chemical equilibrium calculations requires one to define a list of elements to be followed and whose thermodynamic properties will be used in order to calculate the Gibbs free energies needed to find the minimum. Although in principle one might use all the elements available in the CEA library, in this exploratory analysis we wish to focus on the most important elements that condense in the inner part of the disk in order to both avoid numerical errors and speed up computation times. We base our list on important Na, K, Ti, V, and Fe-bearing elements identified in previous works (Lodders 2003, 2010; Moriarty et al. 2014), along with elements present in those that might impact on the final abundances of each of our elements of interest. For example, the feldspar $\text{NaAlSi}_3\text{O}_8$ is the most important Na-bearing condensate and, as such, chemical reactions and condensation of elements involving Al, Si or O also have an impact on the abundance of this condensate. As can be seen, this allows us to follow other elements such as oxygen which in turn will provide us with C/O ratios of gas and solids, given that there are no major carbon condensates in this inner region of the disk.

¹ Fortran code can be obtained at <https://www.grc.nasa.gov/www/CEAWeb/>. A Python wrapper can be found at <http://www.github.com/nespinoza/pyCEA>

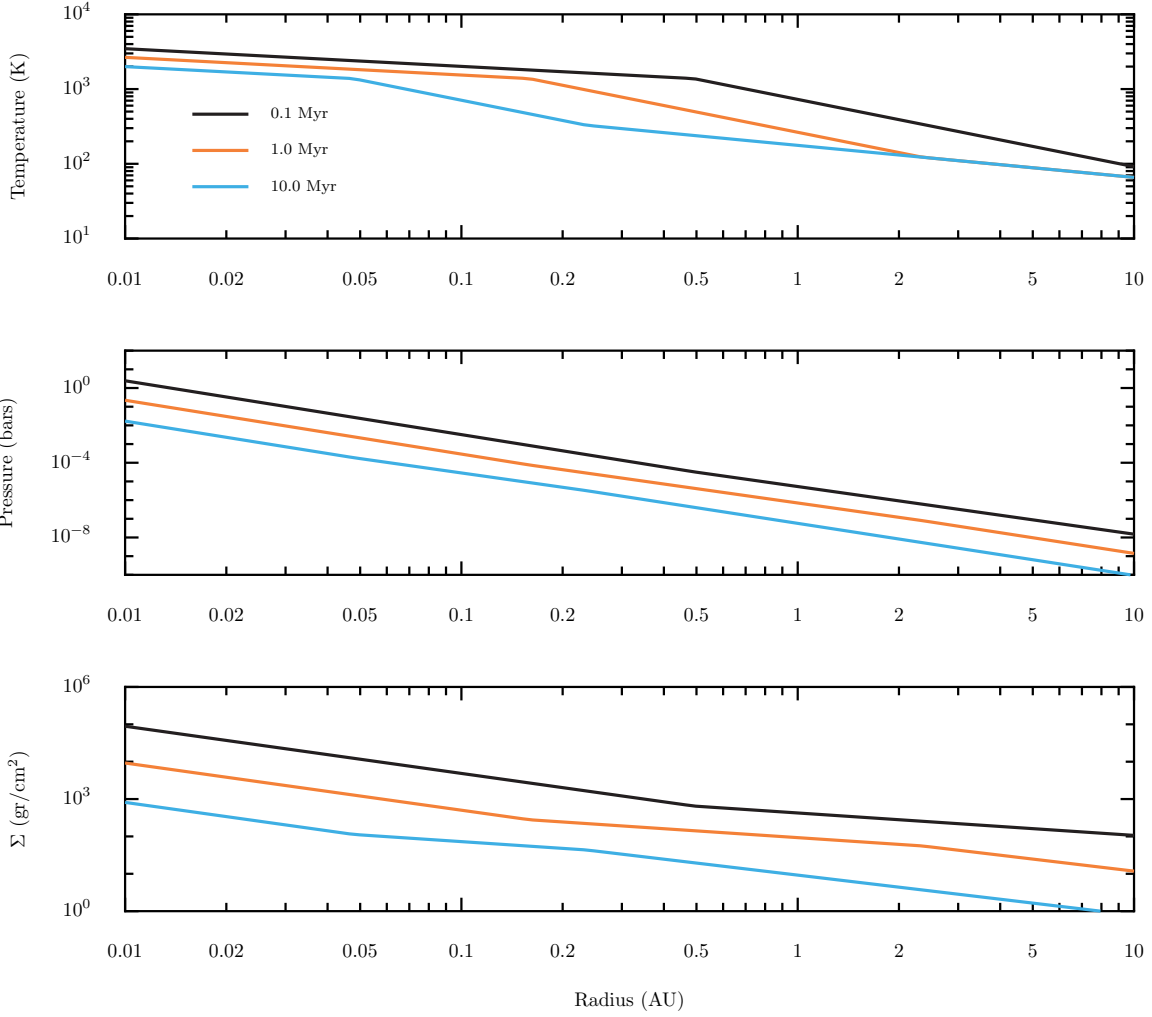


Figure 1. Temperature, pressure and surface density profiles obtained using the [Chambers \(2009\)](#) model for the protoplanetary disk used in this work. The profiles are shown at different times.

Table 2. Species followed on our chemical equilibrium calculations

Gas species					Solid species				
Al	AlN	AlC	AlH	AlH ₂	NaAlSi ₃ O ₈	KAlSi ₃ O ₈	MgAl ₂ O ₄	Al ₂ O ₃	Ca ₂ Al ₂ SiO ₇
AlO	AlOH	AlS	C	CH ₄	Mg ₂ SiO ₄	Fe(α,γ)	FeS(α,β,γ)	CaAl ₁₂ O ₁₉	CaAl ₂ Si ₂ O ₈
CN	CO	CO ₂	CS	Ca	Al	CaTiO ₃	TiN	Ti ₂ O ₃	V ₂ O ₃
CaH	CaO	CaOH	CaH	CaO	Fe ₃ O ₄	MgS	MgSiO ₃		
CaOH	CaS	K	KCN	KH					
KOH	Fe	FeH	FeO	FeS					
Fe(OH) ₂	H	H ₂	H ₂ O	H ₂ S					
HCN	HCO	HS	He	Mg					
MgH	MgN	MgO	MgOH	MgS					
N	N ₂	NH	NH ₃	NO					
Na	Na ₂	NaH	NaO	NaOH					
O	O ₂	OH	S	S ₂					
SN	SO	SO ₂	Si	SiH					
SiH ₄	SiN	SiO	SiS	Ti					
TiO	TiO ₂	TiS	V	VN					

Table 2 continued

Table 2 (*continued*)

Gas species		Solid species
VO	VO ₂	

Table 2 lists the gas and solid species followed in our calculations. The thermodynamic data for most of those species comes from the NIST-JANAF Thermochemical Tables compiled by Chase (1998), and are already included in the CEA thermodynamical library. However, for some gas (FeH, FeS, Fe(OH)₂, HS and TiS) and several solid (NaAlSi₃O₈, KAlSi₃O₈, Ca₂Al₂SiO₇, CaAl₁₂O₁₉, CaAl₂Si₂O₈, FeS(α,β,γ), CaAl₁₂O₁₉, CaAl₂Si₂O₈ and CaTiO₃) species, there is no public thermodynamical data, and data obtained from a database compiled by K. Lodders and B. Fegley was used in order to implement those compounds into this work. The procedures used to fit and implement the data into CEA are explained on Appendix A.

In order to perform chemical equilibrium calculations, the initial abundances of the elements considered needs to be defined. Here we use the proto-solar abundances of the elements from Lodders (2010), assuming they are initially in atomic form. Although this assumption is debatable in general, in our chemical equilibrium calculations it is not important whether the elements were in atomic or molecular form to begin with, specially in the inner regions of the disk under consideration (see, e.g., Eistrup et al. 2016, and references therein).

2.3. Results of the model

In order to obtain the abundances of gas and solid species at each point in the disk at a given time in order to track their evolution, we couple our physical and chemical model for the disk as follows. For a given time, the temperature and pressure at each point in the protoplanetary disk is calculated using our physical model outlined in Section 2.1. Then, at each point on the disk, the temperature and pressure is feeded to the CEA code in order to calculate the equilibrium abundances of each of the species listed in Table 2, as described in Section 2.2. This gives as a result the abundances of each of the compounds as a function of both time and distance in the protoplanetary disk.

Figure 2 illustrates the results of our chemical equilibrium calculations in our time-evolving protoplanetary disk for the V-bearing compounds. As can be observed, because the condensation temperature of vanadium through V₂O₃ is around ~ 1000 K, as the disk cools down this condensation front shifts inwards, where the disk is still hot. At 3 Myr in our disk model, the

disk attains ~ 1000 K at a distance of ~ 0.1 AU from the star in the disk; however, this same temperature is attained at ~ 0.05 AU at 10 Myr. This illustrates nicely how important it is for planetary accretion the fact that we have time-dependant physics and chemistry: at a distance midway between those two points, a planet wouldn't see vanadium in the grains that it is accreting at early stages in the disk, but as the disk cools down, the grains would progressively get more and more vanadium-rich, while the gas would progressively get depleted in it.

In order to illustrate where the different elements under study condense, we track the elemental abundances of each element by considering the molar fractions of the compounds that have these elements and the initial abundances of each of them in order to compute the fraction of each element that is in solid and in gas form in the disk as a function of distance in the disk. The resulting profiles, shown in Figure 3 for a 7 Myr disk, contain very rich information. For example, as expected, the condensation fronts of Na and P occur at almost the same points. However, in our chemical equilibrium calculations, these don't fully condense at these inner regions. This might be a reflection of the fact that the solids that incorporate these elements have a very similar form: while Na goes into NaAlSi₃O₈, K goes into KAlSi₃O₈, and the aluminium, silicates and oxygen-bearing compounds which make those solids are in fact condensing out into different other compounds at those distances. The condensation fronts of Fe and V are also at similar points in the disk, while the Ti condensation front is inwards of those two. Also interesting is the fact that some oxygen (10% – 20%) also gets condensed here mainly in the form of silicates, which in turn enriches the solids in oxygen. Because of this, the C/O ratio of the material in gas form at this time outwards of ~ 0.05 AU in this inner region of the disk is increased, while the ratio of the solid material in the same region is effectively zero because of the fact that there are no important C-bearing solids there.

Our results and positions of the condensation fronts of the elements agree qualitatively with the ones reported on (Lodders 2003), although these can't be directly compared due to the fact that a pressure profile is used in this work which varies by ~ 2 orders of magnitude between 0.01 AU and 0.1 AU, while the work of Lodders

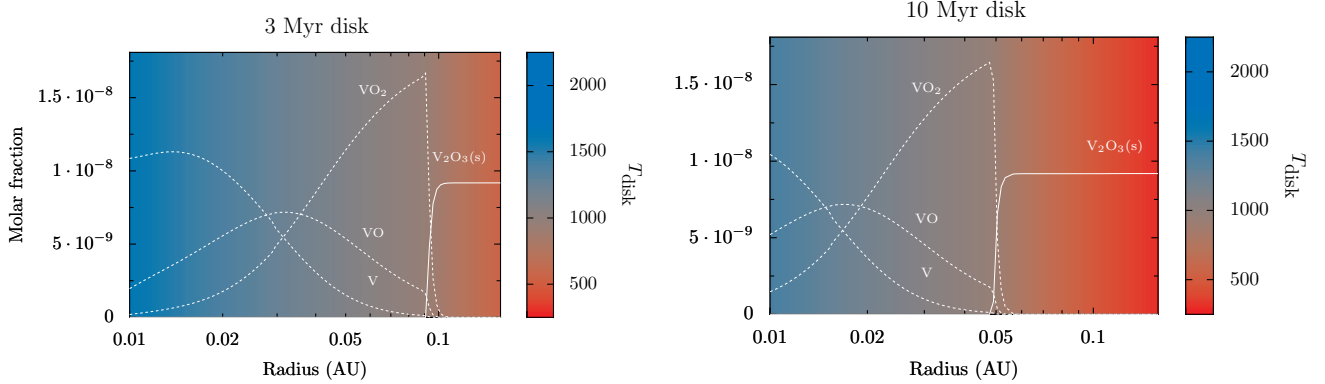


Figure 2. Molar abundance of V-bearing species in both gas (dashed lines) and solid (solid lines) forms in the protoplanetary disk as a function of distance in the inner region of the disk at two different times: 3 Myr (left) and 10 Myr (right). The colorbars indicate the temperature of the disk at the different distances.

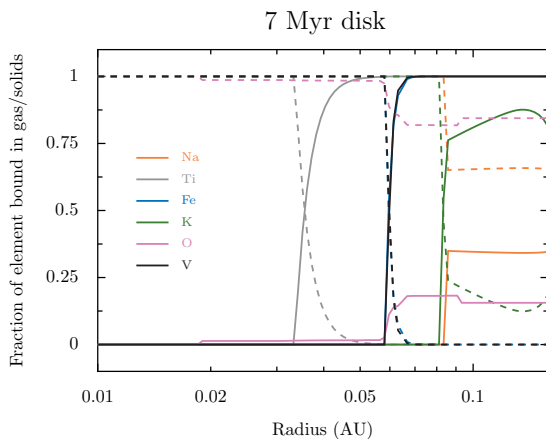


Figure 3. Fraction of the elements under study in the inner region of the disk in solid (solid lines) and gas (dashed line) form at 7 Myr.

(2003) uses a constant pressure of 10^{-4} bars to obtain the condensation temperature of the elements, although with a much richer number of species.

3. PLANETARY ENVELOPE ENRICHMENT

One of the key products of our model is the ability to track the composition of solid and gas material in the disk as a function of both space and time. This is important for “in-situ” planetary accretion, as these planets accrete material during the cooling of the protoplanetary disk in solids and gas in different proportions which, as we observed in the past section, have different enrichment of different elements depending on the age of the disk. In this section we explore how the composition of the envelopes of giant planets accreting material at these inner regions changes depending on the position of the planet.

To illustrate the effect, here we explore planets accreting material in two positions in the disk: a planet accreting its envelope at 0.01 AU, and another one accreting it at 0.05 AU. The first one is of interest given that this is the position in which Na and K partially

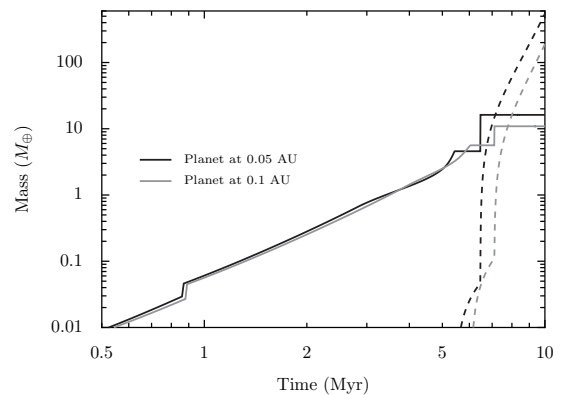


Figure 4. Total mass accreted in solids (solid lines) and gas (dashed lines) for planets starting gas accretion at 0.1 AU (grey lines) and 0.05 AU (black lines).

condense (see Figure 3), and Na and K are one of the major observables in the optical part of the spectrum for giant exoplanets. The second is also of interest as this is the position in the disk at which Ti condenses, an observable in the optical that has also been claimed to be detected.

The planetary formation and gas accretion models used here are described in detail in Miguel & Brunini (2008, 2009, 2010) and Miguel et al. (2011a,b); in brief, planet cores are started to form beyond the ice line in the protoplanetary disk, and we select those planets whose cores migrate at the positions of interest in order to follow their gas and solid accretion history. The gas accretion is on-set after a critical mass is reached (which is similar for the planets explored in this work), and the gas and solid accretion rates are obtained by following the prescriptions described in Miguel & Brunini (2008) and Miguel & Brunini (2009). Once the gas accretion starts, we suppose all the material is added to the envelope and is well mixed. Figure 4 shows the total accreted mass in gas and solids for the planets considered in this work as a function of time, where it can be seen that for both planets, the envelope accretion starts around ~ 6

		Numerator						
		Na	K	Ti	V	Fe	O	C
Denominator	Na	1.00	1.89	2.30	2.30	2.30	0.62	0.31
	K	0.53	1.00	1.22	1.22	1.22	0.33	0.16
	Ti	0.43	0.82	1.00	1.00	1.00	0.27	0.13
	V	0.43	0.82	1.00	1.00	1.00	0.27	0.13
	Fe	0.43	0.82	1.00	1.00	1.00	0.27	0.13
	O	1.62	3.05	3.72	3.72	3.72	1.00	0.50
	C	3.24	6.12	7.45	7.45	7.45	2.00	1.00

Figure 5. Deviation-from-stellar ratios of different elements for the case of the planet accreting the envelope at 0.1 AU. Darker colors imply larger deviations from the stellar values.

Myr.

The exact composition of the accreted gas and solids is the one derived from our chemical equilibrium calculations described in the past section. Here we assume that the composition of the solid and gas material accreted by the planet is the one of the solids and gas at that position at a given time t , i.e., we make the simplifying assumption that there is no strong radial movement of material of composition different than the material at that position in the disk. This in turn implies that at the end, we know the exact composition of the envelope for each of the considered planets. In the next subsections we describe the final composition of those planets.

3.1. Envelope accretion at 0.1 AU

The planet that starts its envelope accretion at 0.1 AU has initially a $5.64M_{\oplus}$ core, and the final accreted envelope has a total mass of $194M_{\oplus}$ ($0.6M_{\text{Jup}}$). From that mass, only $5.3M_{\oplus}$ come from solid material. It is important to note, however, that the metal fraction of the accreted gas material in the envelope is of only $Z = 0.01$ (i.e., the material is heavily hydrogen dominated), while the metal fraction of the accreted solid material is effectively $Z = 1$. This means that the total mass in metals accreted from the gas is of only $1.9M_{\oplus}$, while the total mass in metals accreted from solids is $5.3M_{\oplus}$. This in turn means that the bulk metal content of the accreted envelope actually comes from the solid material and not the gas, implying that if our objective is to look for interesting ratios between elements, we should pay attention to the ratios in the solid material in the protoplanetary disk. From Figure 3, for example, we can tell that, for a planet accreting material at 0.1 AU at 7 Myr, a larger-than-stellar K/Na ratio is expected, be-

		Numerator						
		Na	K	Ti	V	Fe	O	C
Denominator	Na	1.00	1.00	69.59	1.00	1.00	2.25	1.00
	K	1.00	1.00	69.59	1.00	1.00	2.25	1.00
	Ti	0.01	0.01	1.00	0.01	0.01	0.03	0.01
	V	1.00	1.00	69.59	1.00	1.00	2.25	1.00
	Fe	1.00	1.00	69.59	1.00	1.00	2.25	1.00
	O	0.45	0.45	30.97	0.45	0.45	1.00	0.45
	C	1.00	1.00	69.59	1.00	1.00	2.25	1.00

Figure 6. Deviation-from-stellar ratios of different elements for the case of the planet accreting the envelope at 0.05 AU. Darker colors imply larger deviations from the stellar values.

cause a fraction $f_{\text{K,solids}} \sim 0.75$ of the K is in solid form, while only a fraction $f_{\text{Na,solids}} \sim 0.35$ of the Na is in solids, implying that the solids have a K/Na ratio $f_{\text{K,solids}}/f_{\text{Na,solids}} \sim 2$ times larger than the protosolar K/Na ratios which are close, but not exactly equal, to the stellar K/Na ratios. For simplicity, in what follows we refer to those as the stellar ratios.

Figure 5 shows a diagram presenting the deviations-from-stellar ratios on the accreted envelope for our planet. The diagram shows that, as we predicted, the K/Na is 1.89 (~ 2) times larger than the stellar K/Na ratio. However, there are other interesting ratios as well. For example, the Ti/Na, V/Na and Fe/Na ratios of planets accreting envelopes at this position in the protoplanetary disk according to our model have values 2.3 larger-than-stellar. Those are the same because at that position all the Ti, V and Fe is already in solid form. Also interesting is the fact that the C/O ratio in this case is 2 times smaller than the stellar value, which is of course due to the fact that, as discussed on the past section, a small fraction of the oxygen is being condensed into solids: because the solids dominate the overall ratios of the envelope, this oxygen enrichment in the solid material implies a lower-than-stellar C/O ratio. This solid enrichment provides in turn also ratios between oxygen and the other elements around 3 – 4 times larger-than-stellar.

3.2. Envelope accretion at 0.05 AU

For the planet accreting its envelope at 0.05 AU, the initial core has a mass of $4.6M_{\oplus}$, and the final accreted envelope has a total mass of $556.6M_{\oplus}$ ($1.75M_{\text{Jup}}$). Again, from that mass only $11.6M_{\oplus}$ come from solid material, while $545M_{\oplus}$ come from gas. Similar to the

case of the planet accreting material at 0.1 AU, here the ratios are once again dominated by the solid material which provides more than two times more metals than the gas.

In this case we would expect large Ti enrichment in the envelope, due to the fact that most of the titanium is in solid form. Figure 6 shows the corresponding diagram presenting the deviations-from-stellar ratios on the accreted envelope for this planet, where this can be seen. Ratios 70 times larger-than-stellar can be observed for the case of all the elements except for oxygen, where a Ti/O ratio ~ 40 times larger than stellar is observed. Again, the oxygen enrichment of the solid material gives rise to a C/O ratio 0.45 times smaller than the stellar value.

4. DISCUSSION

In the past section, we have showed how our 1D+D physical model of the protoplanetary disk coupled with chemical equilibrium calculations have allowed us to explore different elemental enrichments in the accreted envelopes of giant planets. The question that remains to be answered is whether these can be observed or not with present or future instruments. In order to answer this question, we use the accreted abundances for each planet and use CEA to compute the resulting mixing ratios of the different elements in the atmospheres of these planets by assuming chemical equilibrium. With these, we generate transmission spectra for each of those planets using the methods described in Fortney et al. (2010).

Figure 7 shows the resulting transmission spectra for the two cases explored in this work along with the resulting transmission spectrum that would be observed if the accreted atmosphere had the same abundances as the proto-sun for comparison. As can be seen, for the case of the planet accreting an atmosphere at 0.1 AU, we observe small differences. The largest difference is on the potassium line, were deviations of ~ 50 ppm with respect to an atmosphere accreted with proto-solar abundances is observed. Although this region in wavelength will be observed by JWST and it appears to be detectable in principle given the expected noise properties for observations of giant exoplanet atmospheres (see, e.g., Barstow et al. 2015, and references therein), it appears the challenge of detecting the signature of in-situ accretion could actually be related to disentangling it from other effects, such as broadening of the potassium

line.

The case of an atmosphere accreted at 0.05 AU, on the other hand, looks much more promising. The observed difference with that of a transmission spectrum with proto-solar abundances is of ~ 60 ppm, which is also detectable in principle. On top of this, the potassium line seems not to be affected in this case, and it seems this could be a good reference line in order to search for deviations in the transmission spectrum in this case. However, here the major problem seems to be the ubiquitousness of the TiO/VO features. In particular, TiO has been proposed to not being observable due to cold traps present in the nightsides of giant exoplanets Parmentier et al. (2013).

5. CONCLUSIONS

In this work we have explored the possibility of detecting signatures of “in-situ” accretion in the transmission spectrum of exoplanets. For this, a 1D+D physical model of a protoplanetary disk was coupled with chemical equilibrium calculations and planet formation and accretion models in order to predict the composition of envelopes of giant exoplanets, and the possible observables with present and future instruments such as JWST.

We explored two cases of planets performing “in-situ” accretion: one planet accreting its envelope at 0.1 AU (where, in our models, we observe the Na and K condense) and other accreting its envelope at 0.05 AU (where we observe Ti-bearing condensates appear). Our results suggest that, in principle, the signatures could be detectable, although several issues have to be understood first before claiming evidence for “in-situ” accretion in the transmission spectra of exoplanets. The most promising case appears to be that of a planet at 0.05 AU, where signals of 60 ppm could provide evidence for such accretion mechanism.

N.E. would like to thank the Kavli Summer Program in Astrophysics (KSPA) for providing such a rich experience both from a personal and academic perspective. N.E. would also like to thank K. Lodders and B. Fegley for providing the thermodynamic data used in this work. Funding for the development of this project was provided by KSPA, the Vicerrectoria de Investigacion of the Pontificia Universidad Catolica de Chile (VRI-PUC) and CONICYT-PCHA/Doctorado Nacional.

APPENDIX

A. FITS TO THERMODYNAMIC DATA

The thermodynamic data for each species consisted on tables containing the molar heat capacity at constant pressure, C_p^o , the enthalpy, H^o , and the entropy, S^o , at different temperatures T for each species. Then, fits were done to the

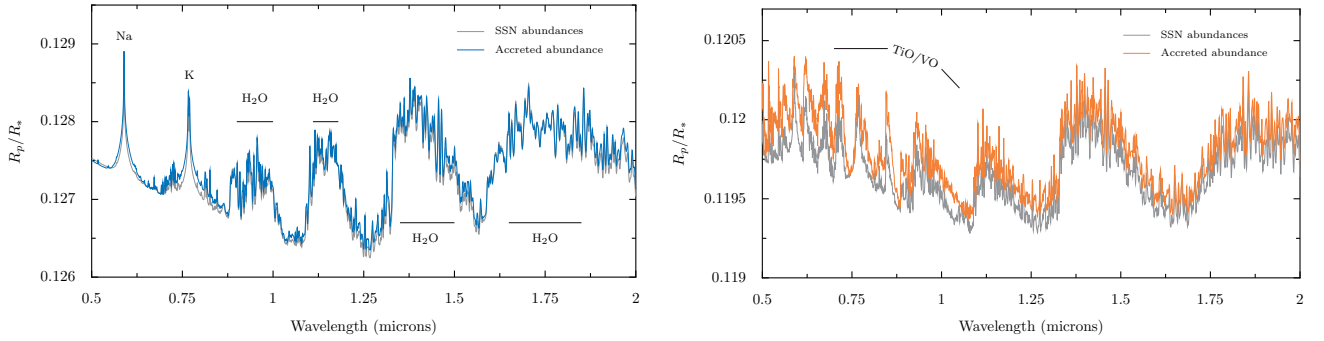


Figure 7. (*Left*) Transmission spectrum assuming accreted “in-situ” abundances at 0.1 AU (blue) and proto-solar abundances (grey) (*Right*) Assuming accreted “in-situ” abundances at 0.05 AU (red) and proto-solar abundances (grey).

data by assuming that C_p^o/R , where R is the gas constant, was of the form

$$C_p^o(T)/R = a_1T^{-2} + a_2T^{-1} + a_3 + a_4T + a_5T^2 + a_6T^3 + a_7T^4,$$

and that $H^o/(RT)$ and S^o/T , as a consequence, were of the form

$$\begin{aligned} H^o(T)/(RT) &= -a_1T^{-2} + a_2T^{-1} \ln(T) + a_3 + a_4T/2 + a_5T^2/3 + a_6T^3/4 + a_7T^4/5 + b_1/T, \\ S^o(T)/T &= -a_1T^{-2}/2 - a_2T^{-1} + a_3 \ln(T) + a_4T + a_5T^2/2 + a_6T^3/3 + a_7T^4/4 + b_2, \end{aligned}$$

where b_1 and b_2 are integration constants. The assumption of these polynomial forms is two-fold; on one hand, this is the expected format by CEA (i.e., CEA expects the coefficients a_i and b_j , with $i = 1, \dots, 7$ and $j = 1, 2$) and, on the other hand, these provide very good fits to the data, with the exception of some solid phases, for which linear fits were sufficiently good. For these, we set a_1 , a_2 , a_5 , a_6 and a_7 equal to zero. In addition, the fits were constrained so that the functions reproduced their values at $T = 298.15$ K exactly, in order for them to reproduce the heat of formation.

In several cases, (one or several) phase transitions were evident in the data as evident discontinuities. At those points, different fits were performed for each phase, but making sure that the difference between the Gibbs free energies at the phase transitions was exactly zero, i.e., if T_{PT} is the temperature at which the phase transition occurs and we denote by H^o and S^o the enthalpy and entropy before the phase transition and \tilde{H}^o and \tilde{S}^o the same thermodynamic quantities after the phase transition the fit, in addition to the above mentioned constraints, is also constrained to give

$$G(T_{PT}) - \tilde{G}(T_{PT}) = 0 \Rightarrow H^o(T_{PT}) - T_{PT}S^o(T_{PT}) - \left[\tilde{H}^o(T_{PT}) - T_{PT}\tilde{S}^o(T_{PT}) \right] = 0$$

exactly. The constrained fits were made using the `lmfit` Python library².

REFERENCES

- Barstow, J. K., Aigrain, S., Irwin, P. G. J., Kendrew, S., & Fletcher, L. N. 2015, *MNRAS*, 448, 2546
- Batygin, K., Bodenheimer, P. H., & Laughlin, G. P. 2015, *ArXiv e-prints*, arXiv:1511.09157
- Boley, A. C., Granados Contreras, A. P., & Gladman, B. 2016, *ApJL*, 817, L17
- Chambers, J. E. 2009, *ApJ*, 705, 1206
- Chase, M. W. 1998, *NIST-JANAF Thermochemical Tables, Fourth Edition, Vol. 9 (Journal of Physical and Chemical Reference Data)*
- Eistrup, C., Walsh, C., & van Dishoeck, E. F. 2016, *ArXiv e-prints*, arXiv:1607.06710
- Evans, T. M., Sing, D. K., Wakeford, H. R., et al. 2016, *ApJL*, 822, L4
- Fortney, J. J., Shabram, M., Showman, A. P., et al. 2010, *ApJ*, 709, 1396
- Henning, T., & Semenov, D. 2013, *Chemical Reviews*, 113, 9016
- Kreidberg, L., Line, M. R., Bean, J. L., et al. 2015, *ApJ*, 814, 66
- Lodders, K. 2003, *ApJ*, 591, 1220
- . 2010, *Exoplanet Chemistry*, ed. R. Barnes, 157
- Madhusudhan, N. 2012, *ApJ*, 758, 36
- Madhusudhan, N., Harrington, J., Stevenson, K. B., et al. 2011, *Nature*, 469, 64
- Miguel, Y., & Brunini, A. 2008, *MNRAS*, 387, 463
- . 2009, *MNRAS*, 392, 391
- . 2010, *MNRAS*, 406, 1935
- Miguel, Y., Guilera, O. M., & Brunini, A. 2011a, *MNRAS*, 417, 314
- . 2011b, *MNRAS*, 412, 2113
- Moriarty, J., Madhusudhan, N., & Fischer, D. 2014, *ApJ*, 787, 81
- Öberg, K. I., Murray-Clay, R., & Bergin, E. A. 2011, *ApJL*, 743, L16

² <https://lmfit.github.io/lmfit-py/>

ALL AUTHORS AND AFFILIATIONS

AND

NÉSTOR ESPINOZA^{1,2}, JONATHAN J. FORTNEY³, YAMILA MIGUEL⁴.

¹Instituto de Astrofísica, Facultad de Física, Pontificia Universidad Católica de Chile, Av. Vicuña Mackenna 4860, 782-0436 Macul, Santiago, Chile.,

²Millennium Institute of Astrophysics, Av. Vicuña Mackenna 4860, 782-0436 Macul, Santiago, Chile.,

³Department of Astronomy and Astrophysics, University of California, Santa Cruz, USA.,

⁴Laboratoire Lagrange, UMR 7293, Université de Nice-Sophia Antipolis, CNRS, Observatoire de la Côte d'Azur, Blvd de l'Observatoire, CS 34229, 06304 Nice cedex 4, France.